Inorganic Chemistry

ARTICLE

pubs.acs.org/IC

Syntheses and Photophysical Properties of Luminescent Mono-cyclometalated Gold(III) *cis*-Dialkynyl Complexes

Jai Anand Garg, Olivier Blacque, and Koushik Venkatesan*

Institute of Inorganic Chemistry, University of Zürich, Winterthurerstrasse 190, CH-8057 Zürich, Switzerland

Supporting Information

ABSTRACT: A series of novel luminescent neutral cyclometalated gold(III) complexes of the type *cis*-[(N^C)Au(C≡CR)$_2$] (R = aryl, silyl groups) having different cyclometalating cores (N^C) have been synthesized by CuI promoted halide to alkynyl metathesis with NEt_3 as in situ deprotonating agent. Along with spectroscopic characterizations (nuclear magnetic resonance and infrared spectroscopies and electrospray ionization mass spectrometry) and elemental analysis, the molecular structures of some of the complexes have been established by single-crystal X-ray diffraction studies. Photophysical studies reveal that the complexes exhibit room-temperature phosphorescence (RTP). Experimental observations and density functional theory calculations qualitatively suggest limited participation of the metal and alkynyl ligands in the lowest energy emitting state. The nature of the emission is mainly governed by metal-perturbed ^{3}IL($\pi-\pi^*$) transitions originating from the cyclometalate part of the molecule, and its variation readily leads to the tuning of the emission wavelengths. Cyclic voltammetry measurements of selected complexes showed irreversible redox behavior with near-equivalent cathodic peak potential ($E_{p,c}$) assigned to the C^N core.

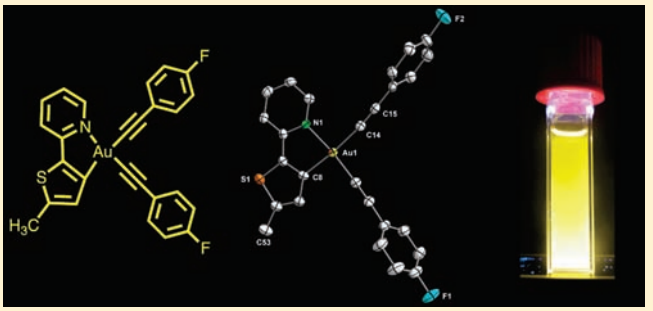

INTRODUCTION

Organogold(I) σ-alkynyl complexes are widely investigated for their interesting luminescence, nonlinear optical (NLO) properties and their ability to build metallo-macromolecular entities.[1−9] In sharp contrast, gold(III) alkynyl complexes are relatively less explored. Notables among the few known examples include mononuclear gold(III) complexes containing one alkynyl ligand, viz., [Au(C≡CCF$_3$)Me$_2$(L)] and [Au(C≡CR)Me$_2$(PPh$_3$)],[10,11] [Au(C^N^C)(C≡CR)],[2,12,13] and three alkynyl ligands [Au(C≡CR)$_3$(L)] and four alkynyl ligands [ER$_4$]$^+$[Au(C≡CR)$_4$]$^-$.[14,15] Dinuclear gold(I)−gold(III) complexes bearing two alkynyl ligands, viz., [Au^I(μ-{CH$_2$}PPh$_2$)$_2$Au^{III}(C≡CR)$_2$], have also been reported[16] (Figure 1). In general, gold(III) complexes tend to exhibit relatively large positive reduction potentials,[17,18] and the consequent instability is a probable reason for their scarcity. Except for the cyclometalated systems (C^N^C) in the above-noted examples that have been studied for luminescence properties, the other gold alkynyls have been chiefly explored, either for catalysis or for studying reductive elimination processes.[10,11,14,15] In recent years, extensive investigations carried out by Yam and co-workers has revealed that cyclometalated gold(III) monoalkynyl complexes with terdentate ligands can exhibit room-temperature phosphorescence.[2,12,13] Also, external quantum efficiency (EQE) to the order of 11.5% in an organic light emitting diode (OLED) device which is well comparable to cyclometalated Ir(III) systems has been achieved.[19]

In the past few years, we have been interested in a relatively less explored class of mononuclear cyclometalated neutral diaryl/dialkynyl gold(III) complexes. Gold(III) alkynyls, similar to isoelectronic platinum(II) alkynyl systems (d^8-configuration) could possibly offer tunable electronic and luminescent properties due to their electron-richness, rigid-rod nature, and polarizability.[8,20] In our previous study, we have shown that diaryl complexes of the type *cis*-[(N^C)AuL$_n$] (L = aryl, n = 1, 2) containing perfluorinated aryl groups can be quite stable and offer interesting photophysical properties.[21] Very recently, investigations into gold(III) dialkynyl systems have appeared in literature further exemplifying their importance.[22]

From a photophysical standpoint, anionic acetylenic carbon ($^-$C≡) is desirable since strong σ-donating ligands are required for "lifting" the energy levels of the otherwise low-lying metal-centered (MC) orbitals. These orbitals are quite susceptible for thermal population at ambient temperatures which then follows rapid nonradiative relaxation pathways.[2] Here in this work we report the syntheses of stable mononuclear cyclometalated *cis*-gold(III)-σ-dialkynyl complexes and their luminescent properties.

RESULTS AND DISCUSSION

Syntheses and Characterization of Complexes. Dichlorogold(III) complexes (**A**−**E**) with different cyclometalating cores **1**−**5** (Scheme 1) were first prepared as precursors to obtain the desired dialkynyls. Complex [(N^C)AuCl$_2$] [N^C = 2-phenylpyridine

Received: November 4, 2010
Published: May 23, 2011

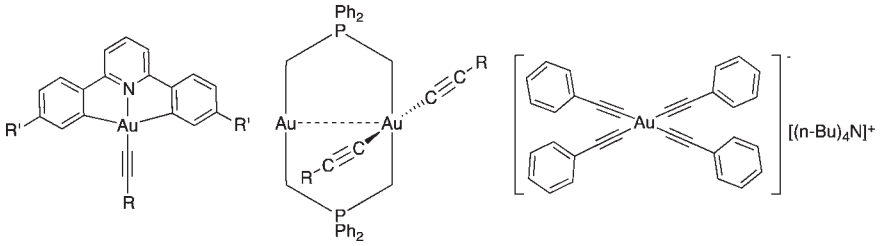

Figure 1. Known gold(III) mono-, di-, and tetraalkynyl complexes.

Scheme 1

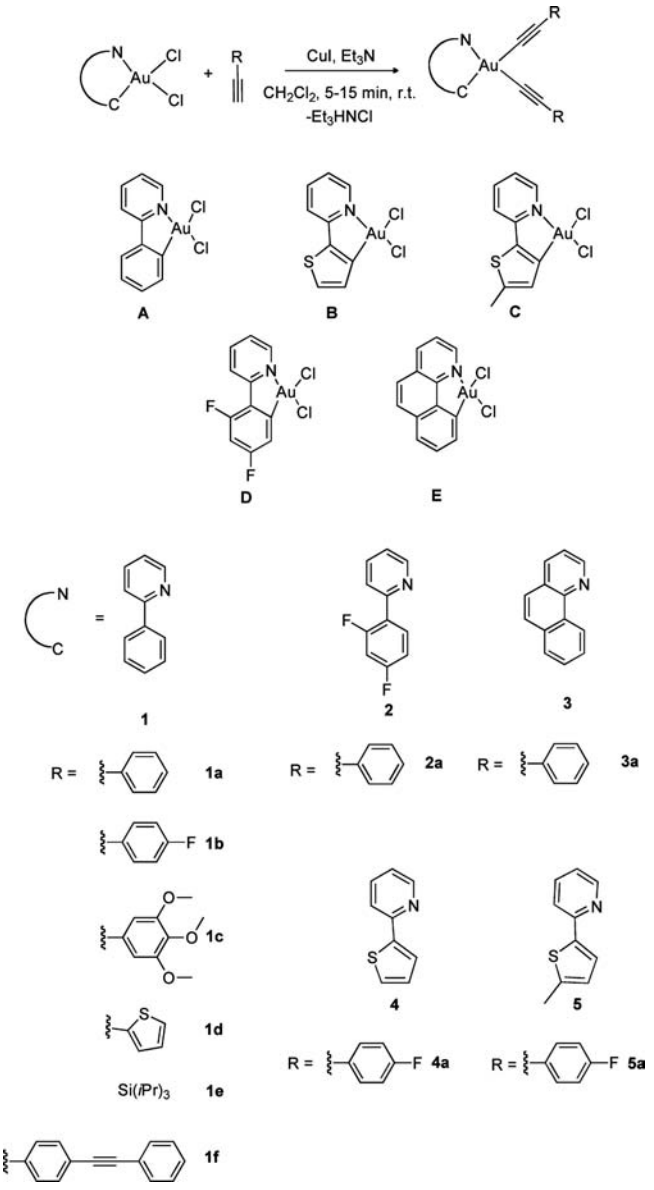

(ppy)] (**A**) was prepared according to the procedure reported by Constable and Leese involving transmetalation reaction of ortho-activated ppyHg^{II} chloride with sodium tetrachloroaurate,[23] [(N^C)-$AuCl_2$] [N^C = 2-(2-thienyl)pyridine (thpy); **B**] and [N^C = 2-(5-methyl-2-thienyl)pyridine (5-me-thpy)][$AuCl_2$; **C**] were synthesized on the basis of direct cycloauration methods.[21,24] The remaining precursor dihalides which were unknown, namely, [(N^C)$AuCl_2$] [N^C = 2-(2,4-difluorophenyl)pyridine (dfppy); **D**] and [(N^C)-$AuCl_2$] [N^C = benzo[*h*]quinoline (bzq); **E**], were prepared via analogous[25,26] literature known transmetalation sequences from mercury derivatives. The method essentially takes advantage of the propensity of mercury(II) salts toward electrophilic substitution for attaining ortho-activation. The ortho-mercurated dfppy was obtained in rather low yield of 11% after repeated recrystallization from ethanol (see Supporting Information for step 1 of **D**). A single resonance signal in ^{199}Hg NMR at $\delta = -1000$ ppm coupled to fluorine $^4J_{Hg-F}$ (248.0 Hz) was observed; the same coupling constant to mercury nucleus was observed in ^{19}F NMR, which showed two sets of signals at −108.3 and −110.1 ppm. A characteristic IR absorption at 342 cm^{-1} assignable to ν(Hg−Cl) was also found. These preceding observations unambiguously establish the identity of the expected ortho-activated [(dfppy)Hg^{II}Cl] and ruled out the possibility of any multiple mercuration which is sometimes encountered in this chemistry.[25,26] Transmetalation of ortho-mercurated bzq (see Experimental Section) required long reaction times (4 days) under optimized conditions of reflux in a 1:1 mixture of dichloromethane and acetonitrile. The ^{1}H NMR spectra of the aurated dichlorides **D** and **E** showed diagnostic downfield shifts (mean difference ($\Delta\delta$), ca. 2.0 ppm) for aromatic proton attached to carbon α to N of the pyridyl ring when compared to those of their respective free dfppy and bzq. In addition IR spectra showed two characteristic stretching vibrations ν(Au−Cl) in the region of 300−415 cm^{-1}.

Utilizing the above precursor complexes, various gold(III) dialkynyls of the type [Au(C^N)(C≡CR)$_2$] [N^C = ppy, R = phenyl (**1a**), 4-fluorophenyl (**1b**), 3,4,5-trimethoxyphenyl (**1c**), 2-thienyl (**1d**), Si(*i*Pr)$_3$ (**1e**), 4-(phenylethynyl)phenyl (**1f**); N^C = dfppy, R = phenyl (**2a**); N^C = bzq, R = phenyl (**3a**); N^C = thpy, R = 4-fluorophenyl (**4a**); and N^C = 5-me-thpy, R = 4-fluorophenyl (**5a**)] were synthesized (Scheme 1). Et_3N served as a mild enough base for in situ deprotonation of the relatively acidic acetylenic proton, and the substitution was aided with the addition of a catalytic amount of CuI. It is pertinent to mention here that Yam et al. have recently reported the synthesis of the same class of compounds by a lithiation protocol.[22a]

The reaction proceeds smoothly to completion in less than 20 min at room temperature (RT). Generally, products were obtained in modest yields (25−60%) following simple workup and flash-column purification using neutral Al_2O_3. Longer reaction times, especially for complexes with thienyl C^N units **4a** and **5a**, lead to an increased amount of unidentified impurities. In the case of **1e**, the reaction was notably clean and complete within 5 min. This could well be expected in light of investigations upon various silyl acetylenes having similar deprotonation rates as compared to aryl acetylenes despite the electronegativity considerations of silicon and carbon.[27] All of the products were completely characterized by ^{1}H, ^{13}C, and ^{19}F NMR and IR spectroscopies and elemental microanalyses. ^{1}H and ^{13}C NMR

dx.doi.org/10.1021/ic102216v |*Inorg. Chem.* 2011, 50, 5430–5441

of all complexes showed two sets of resonances due to the nonequivalent alkynyl ligands. The shift of the proton α to the nitrogen of the pyridyl ring appeared in the range δ = 9.34−9.81 ppm. The higher end values of this interval were notably observed for complexes with bzq and dfppy cores. Such shifts have also been noted with benzoquinoline platinum(II) dialkynyl cyclometalated complexes described in the literature.[28] From the ^{1}H−^{1}H and ^{1}H−^{13}C COSY experiments done for **2a**, the aurated carbon Au−C(sp^2) appeared at 159.0 ppm, which falls in the range previously observed in the literature for five-membered gold(III) metalacycles containing N as one of the donor atoms.[29] Although the chemical shifts for the metalated α-acetylenic carbons ($\delta C_\alpha\equiv$) could not be assigned with certainty, the two C_β signals were observed at δ = 99.0 and 104.0 ppm. In the cases of benzoquinoline platinum(II) dialkynyls the C_α have been unambiguously identified by taking advantage of ^{195}Pt satellites. IR spectra of the prepared complexes showed the expected two acetylenic bands ν(C≡C) characterized by weak absorption in the region of 2100−2200 cm^{-1}.

Stability and Thermogravimetric Studies. During the initial stages of the study, examination of the emission properties of complexes **1a** and **1b** showed no marked variation, and this prompted us to prepare complexes with varied cyclometalating ligands. We chose to use fluorinated aryl acetylides in most of the complexes, with an anticipation they will improve the stability of the complexes on similar lines of thought as explained for gold(III) biaryl complexes presented in our previous study.[21] All complexes synthesized were found to be stable to air and moisture in the solid state under ambient conditions. Homocoupled products, namely, the butadiynes formed through reductive elimination, were observed as byproduct (confirmed by ^{1}H NMR and GC-MS studies) in some cases such as for **1a** and **3a** but were not observed in others, especially for the fluorinated analogues. In comparison with the gold(III) diaryl complexes,[21] these complexes exhibit enhanced stability which could be partly understood on the basis of hybridization considerations of Au−C(sp) vs Au−C(sp^2).

It was interesting to note that while **1c** containing electron-rich alkynyl was quite stable both in solid state and in organic solvents, a dichloromethane solution of **1d** showed discernible decomposition in a few days, and attempts to isolate a complex with 4-ethynyl-*N*,*N*-dimethylaniline as an ancillary ligand with a ppy core (**1**) was unsuccessful because of its instability. Thermogravimetric analysis (TGA) of **1a** and **1b** showed the final decomposition temperature (T_d) of the latter occurs at a much higher temperature around 500 °C than the former at around 290 °C (see Supporting Information Figure S1). This can be probably attributed to the resulting increase in the stability of the complex due to the electron withdrawing nature of fluorine.

Structural Characterization. Single-crystal X-ray structures were determined for seven complexes (**1a**−**1c**, **1e**, **3a**, **4a**, and **5a**). They were obtained from slow evaporation by layering of pentane over concentrated solution of the complexes in dichloromethane at 0−5 °C. The perspective views of **1a**, **1e**, **3a**, and **5a** are shown in Figure 2 (for others, see Supporting Information, Figures S2−S4), and some relevant bond distances and angles are given in Table 1. Crystallographic details are provided in the Supporting Information (Table S1 and Table S2). The structural analysis indicates the coordination environment around the gold metal center as a distorted square-planar geometry which is generally observed for square-planar d^8 complexes with non-equivalent coordination environment. The cyclometalated part is essentially flat, and the largest deviations from the main plane defined by the C^NAuCC metallacycle atoms were 0.072(1) Å observed for **1b** and 0.063(9) Å for **1e**. The maximum twist angle between the planes comprising N^CAu and AuCC was 5.85(14)° in **1b**. The metalated Au−C(sp^2) distances, irrespective of different cyclometalating cores were found to lie in a narrow range of 2.027(3)−2.067(2) Å without much deviation from those reported for their precursor dihalides and other analogous complexes. The N−Au−C_{aryl} chelate bite angles of the complexes were found to range between 80.33(9) and 81.93(9)° with the consequent enlargement of the opposite $C_{alkynyl}$−Au−$C_{alkynyl}$ angle which falls in the range of 88.47(6)−95.28(14)°. The deviation from the idealized 90° is commonly observed in related systems[21,22] and can be attributed to the steric requirements of the cyclometalating ligands. For complexes **1a**−**1c**, **4a**, and **5a** the Au−$C_{alkynyl}$ distances trans to nitrogen of the pyridyl ring lie in the range of 1.965(3)−2.006(2) Å while the distances to other metalated acetylenic carbon fall in the range of 1.993(2)−2.052(2) Å, and this slight but distinct variation could be understood due to the greater trans influence exerted by C(sp^2); however, for complexes **1e** and **3a** the distances were nearly the same within the limits of experimental uncertainty. Deviations from collinearity in the range of 168.2(2)−179.6(3)° were observed for the interatomic angles comprising Au−$C_\alpha\equiv C_\beta$ trans to both N and the metalated carbon. The other angles connecting the aryl or silyl part ($C_\alpha\equiv C_\beta$—$C_{aryl/silyl}$) however did not show large variations. The intermolecular Au···Au distance for **1c** (3.7285(1) Å) was found to be the shortest among the others, which fall in the range of 4.1468(2)−7.6181(1) Å (see Supporting Information Table S3). Since the Au···Au distances are no shorter than the sum of the van der Waals radii between the gold atoms in the crystal lattice, significant aurophilic interactions could be ruled out.

UV−Vis Absorption Studies. The UV−vis profiles of the complexes (see Figure 3 and in Supporting Information Figure S5) with ppy cyclometalate (**1a**−**1f**) and also **2a** exhibit a low-energy absorption band centered around 317−323 nm. Thpy-cyclometalated complex (**4a**) and 5-me-thpy (**5a**) featured bands at lower energies of 368 and 381 nm, respectively, due to their inherent internal charge-transfer nature.[30,31] Understandably, π-delocalization causes lower energy absorptions of bzq (**3a**) at 383 nm. Typically, the complexes showed molar absorptivities in the order of 10^3 to 10^4 dm^3 mol^{-1} cm^{-1}, notably greater in the case of **1f**. In general, the shape of the absorption bands resembled those of the respective free ligands with bathochromic shifts due to metal coordination.

Emission Studies. Complexes except **1c** and **1d** showed intense long-lived phosphorescence at RT. While **1d** showed weak emission at RT (not shown in figures), **1c** was non-emissive (not shown in figures). Nevertheless, all of the complexes showed emission at 77 K (me-THF) rigidified media (see Supporting Information Figure S6). The non-emissive nature of **1c** could be because of thermal equilibrium with deactivating excited states or due to photoinduced electron transfer, presumably from the electron rich methoxy substituents. The latter phenomenon with methoxy-phenylacetylene ligands was also observed previously with Pt(II) cyclometalated complexes.[32] Further studies are due for definitive conclusions. As mentioned earlier, with initial observation that **1a** and **1b** emitting at nearly the same wavelengths (see Table 2), we also thought that either extending the conjugation or changing the cyclometalated ligand can offer tuning of emission wavelengths. Accordingly, **1f** and **2a**−**5a**

dx.doi.org/10.1021/ic102216v |*Inorg. Chem.* 2011, 50, 5430–5441

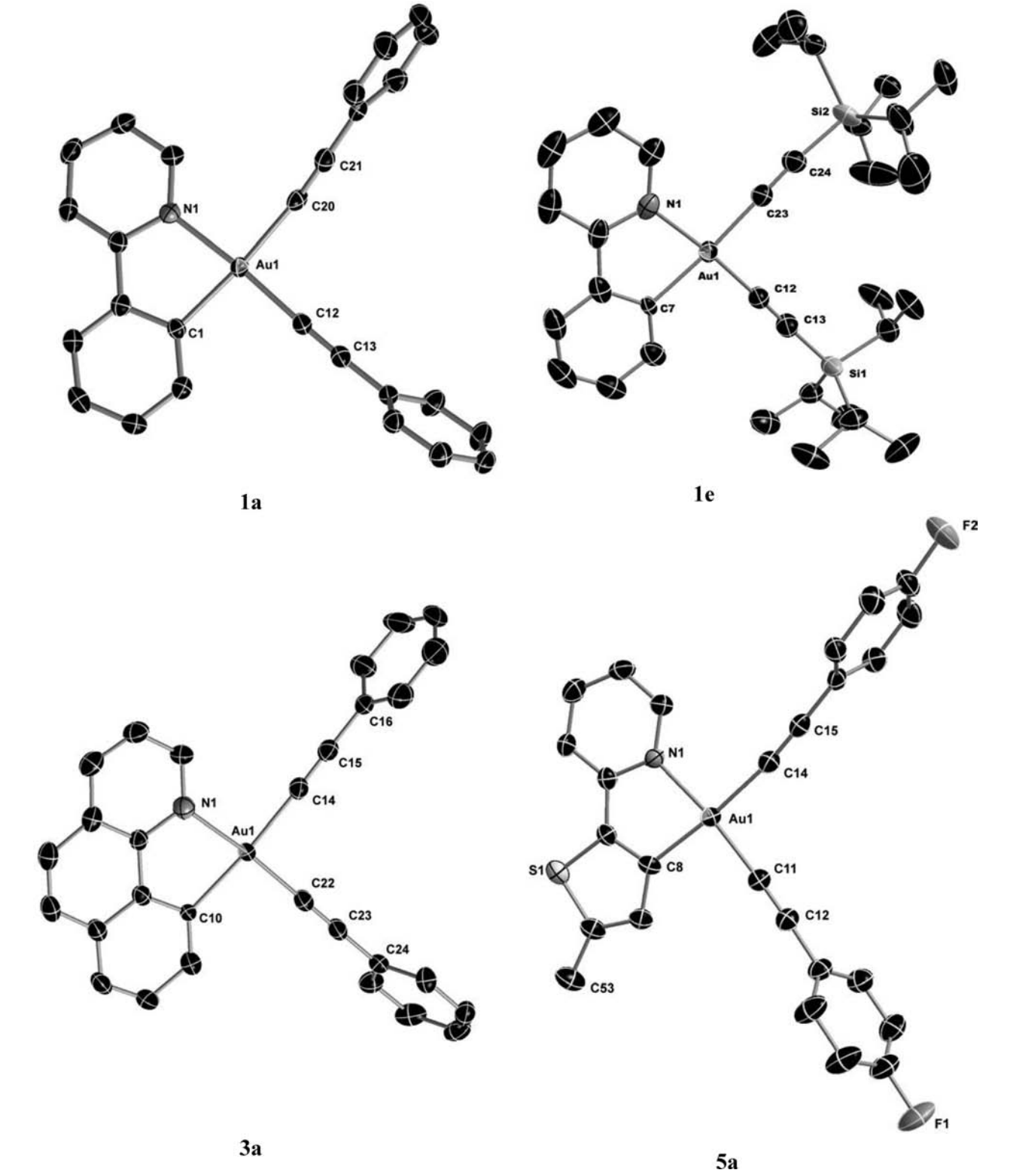

Figure 2. X-ray crystal structures of **1a**, **1e**, **3a**, and **5a** with selective atomic numbering scheme. Thermal ellipsoids are drawn at the 50% probability level. Hydrogen atoms and solvent molecules are omitted for clarity.

did show variation in their lowest energy emission maxima. Interestingly, the structural variation of the cyclometalate such as in **4a** and **5a** was more efficient in tuning emission toward longer wavelengths than that achieved by increasing conjugation by one alkyne unit in the ancillary ligand, such as in **1f**. This suggests the enhanced participation of cyclometalate in the excited state and emission tuning could be achieved by the choice of cyclometalated unit with different $\pi-\pi^*$ energies.

dx.doi.org/10.1021/ic102216v |*Inorg. Chem.* 2011, 50, 5430–5441

Vibrational structured emission profiles even at RT strongly suggest ligand centered (^{3}IL) dominance as in most cases of luminescent gold(III) complexes.[2,12] Emission spectra measured at 77 K generally featured strong bands with vibrational progressions of 1200−1250 cm^{-1} due to the participating ligands (see Supporting Information Figure S6). These values relate more closely to C═N and C═C stretching frequencies and to rocking aromatic C−H modes. Vibrational progressions corresponding to ν(C≡C) stretching modes around 2200 cm^{-1} were comparatively less prominent. No significant residual fluorescence from the ligands was observed in these complexes. It is worth mentioning here that the emission of the fluorescent chromophore benzo[*h*]quinoline λ_{em} = 363 nm shifted to 488 nm in **3a**. The quantum yields (Φ_p) were generally found to lie in the order of 10^{-2} and were notably greater for **1e**; this is also qualitatively in agreement with the quantum yield values observed for Au(III) complexes described recently in literature.[22] As anticipated, there was an increase in the quantum yield of **3a** as compared to **1a**, which could be explained in terms of a partial decrease in nonradiative decay rates (k_{nr}) due to structural rigidification. The decrease in quantum yield of **5a** as compared to **4a** could be understood on the basis of the excited-state structural distortions associated with complexes accompanying a larger Stokes shift. Utilization of dfppy ligand **2**, popular for blue emission in Ir(III)[33] and Pt(II)[34] complexes in **2a**, did show a hypsochromic shift of 8 nm as compared to **1a**. Longer emission wavelengths of **5a** as compared to that of **4a** are due to the lowering of the $\pi-\pi^*$ band gap consequent from the increased electron richness of the thienyl unit. The Stokes shift for these complexes are large, and the excited-state lifetime is in the microsecond regime, indicating the phosphorescent nature of emission. Considering the above observations, and also from the longer excited-state lifetimes (τ), in line with the increasing internal charge-transfer nature of the C^N unit, **5a** > **4a** > **2a**, the emission is assigned to originate from the ^{3}IL ($\pi-\pi^*$) state of the cyclometalate perturbed by the metal.

Table 1. Selected Bond Distances (Å) and Angles (deg) Data of Complexes 1a, 1e, 3a, and 5a

	distance		angle
		Complex **1a**	
C(12)−Au(1)	1.971(2)	C(1)−Au(1)−N(1)	81.33(9)
C(20)−Au(1)	2.052(2)	C(12)−Au(1)−C(20)	90.39(9)
C(1)−Au(1)	2.038(2)	C(1)−Au(1)−C(12)	94.19(9)
N(1)−Au(1)	2.0596(19)	N(1)−Au(1)−C(20)	94.09(8)
		Complex **1e**	
C(7)−Au(1)	2.052(2)	C(7)−Au(1)−N(1)	80.33(9)
N(1)−Au(1)	2.0515(19)	C(23)−Au(1)−C12	89.93(9)
C(23)−Au(1)	1.993(2)	C(23)−Au(1)−N(1)	94.99(9)
C(12)−Au(1)	2.006(2)	C(12)−Au(1)−C(7)	94.75(9)
		Complex **3a**	
C(10)−Au(1)	2.067(2)	N(1)−Au(1)−C(10)	81.93(9)
N(1)−Au(1)	2.061(2)	C(22)−Au(1)−C(14)	92.64(10)
C(14)−Au(1)	2.008(3)	C(14)−Au(1)−N(1)	92.25(9)
C(22)−Au(1)	2.003(3)	C(22)−Au(1)−C(10)	93.14(9)
		Complex **5a**	
N(1)−Au(1)	2.082(2)	C(8)−Au(1)−N(1)	81.07(10)
C(8)−Au(1)	2.032(3)	C(11)−Au(1)−C(14)	92.61(11)
C(14)−Au(1)	2.040(3)	C(14)−Au(1)−N(1)	94.16(10)
C(11)−Au(1)	1.965(3)	C(11)−Au(1)−C(8)	92.20(11)

Cyclic Voltammetry Studies. Cyclic voltammetry for selected complexes **1a**−**1c**, **1f**, **4a**, and **5a** (see Supporting Information Table S4) showed irreversible oxidation peaks in the range from +0.29 to +0.70 V (vs Fc$^{0/+}$ couple) and irreversible cathodic peak potentials in the range from −2.29 to −2.48 V (vs Fc$^{0/+}$ couple) in CH_2Cl_2 at RT. Both processes are assignable to ligand-centered electrochemical events. Due to the similarity of the reduction peak potentials within the same C^N cyclometalate, the reduction process is attributed to origination from the cyclometalated part of the complex and the oxidation from the electron rich alkynyl unit. On the basis of precedences of CV studies of related complexes,[12,22,35] and due to the oxidizing nature of the gold(III) complexes, the metal is less likely to be involved in the redox process. The large electrochemical band gap with oxidation and the reduction peaks widely separated, along with the absence of redox activity from the metal, further corroborates our photophysical observation of the limited participation of the metal in the frontier orbitals.

Density Functional Theory and Time-Dependent Density Functional Theory Calculations. To better understand the absorption and emission properties of the synthesized compounds, density functional theory (DFT) calculations were carried out for selected molecules with the Gaussian 03 program package.[36] The

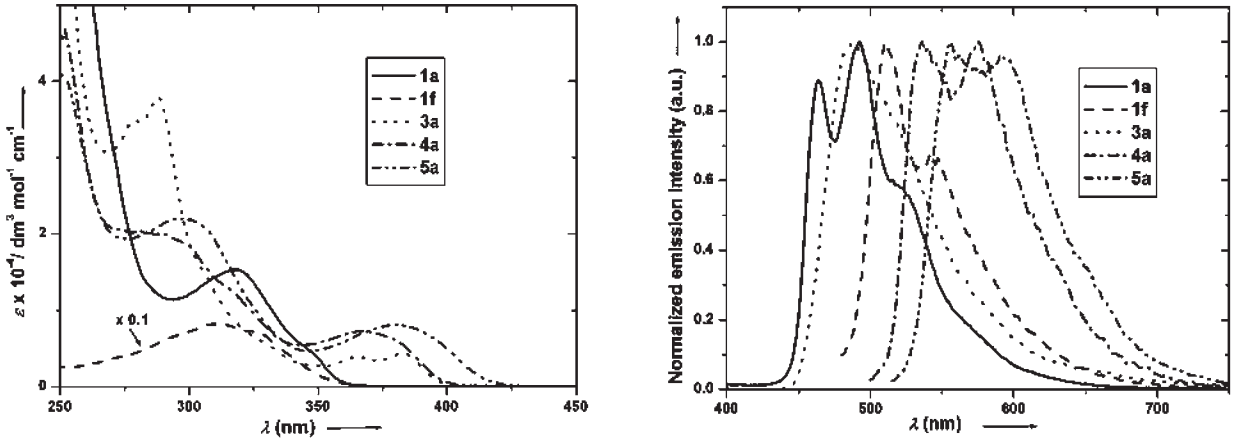

Figure 3. (Left) Electronic absorption spectra in CH_2Cl_2 at RT and (right) normalized emission (*I*) spectra in degassed CH_2Cl_2 at RT.

dx.doi.org/10.1021/ic102216v |*Inorg. Chem.* 2011, 50, 5430–5441

Table 2. Photophysical Properties of Complexes 1a−1f and 2a−5a

	room-temperature solution (CH_2Cl_2)				
complex	absorption λ_{max} (nm; ε_{max}/(dm^3 mol^{-1}cm^{-1}))	emission λ_{max} (nm)	τ (μs)	Φ_p [a]	77 K glass[b] (2-me-THF; nm)
1a	318 (15 310)	463, 491, 524 sh	4.4	6.0×10^{-3}	457, 491, 518
1b	318 (13 681)	467, 493, 526 sh	4.5	4.0×10^{-2}	456, 490, 522
1c	321 (15 340)	non-emissive			458, 492, 520
1d	261 (21 290), 323 (10 551)	weakly emissive			486, 505, 525
1e	250 (22 394), 319 (8550), 341 sh (5278)	461, 492, 521 sh	1.4	0.11	459, 486, 528
1f	310 (82 244), 327 sh (71 261)	510, 542	13.0	5.9×10^{-2}	502, 533, 563
2a	317 (1825)	462, 483	1.4	1.6×10^{-2}	457, 522, 555
3a	289 (38 030), 365 (3910), 383 (4374)	488, 515 sh	11.2	1.2×10^{-2}	487, 520
4a	281 (20 314), 368 (7320)	534, 575	7.4	4.4×10^{-2}	452, 574, 590
5a	295 (21 950), 381 (8120)	556, 591	19.1	1.5×10^{-2}	545, 570, 598

[a] Photoluminescence quantum yield determined with quinine sulfate in 1 N H_2SO_4 as standard at 298 K. [b] Vibronic structured emission bands.

Table 3. Selected Singlet−Singlet (S_0-S_n) and Singlet−Triplet (S_0-T_m) Excited States with TDDFT/CPCM Vertical Excitation Energies (nm), Transition Coefficients, Orbitals Involved in the Transitions, and Oscillator Strengths *f* for Compounds 1a, 1b, 1e, and 4a (with $f > 0.015$)

	1a	**1b**	**1e**	**4a**
exp abs λ_{max}	318	318	319	368
S_0-S_n	$n = 3$	$n = 2$	$n = 1$	$n = 1$
	318 (0.175) H-2 → L (0.67)	339 (0.083) H-1 → L (0.66)	323 (0.079) H → L (0.63)	353 (0.038) H → L (0.62)
S_0-S_n	$n = 4$	$n = 3$	$n = 4$	$n = 2$
	292 (0.192) H-3 → L (0.65)	318 (0.182) H-2 → L (0.67)	302 (0.150) H-3 → L (0.64)	351 (0.138) H-2 → L (0.57)
S_0-S_n	$n = 6$	$n = 4$	$n = 5$	$n = 3$
	278 (0.123) H → L+2 (0.53)	292 (0.181) H-3 → L (0.65)	299 (0.215) H-4 → L (0.63)	337 (0.267) H-1 → L (0.68)
S_0-S_n	$n = 7$	$n = 6$	$n = 7$	$n = 5$
	276 (0.032) H-6 → L (0.45)	280 (0.054) H-4 → L (0.65)	274 (0.139) H → L+1 (0.58)	293 (0.199) H-3 → L (0.68)
S_0-S_n	$n = 8$	$n = 7$		$n = 7$
	276 (0.034) H-1 → L+1 (0.46)	280 (0.028) H-1 → L+2 (0.61)		290 (0.248) H → L+2 (0.57)
S_0-S_n	$n = 9$	$n = 8$		$n = 8$
	274 (0.311) H-1 → L+2 (0.50)	275 (0.291) H → L+2 (0.64)		284 (0.059) H → L+1 (0.60)
S_0-S_n	$n = 10$	$n = 9$		$n = 9$
	265 (0.143) H-7 → L (0.44)	273 (0.051) H-1 → L+1 (0.63)		284 (0.133) H-2 → L+1 (0.54)
S_0-S_n		$n = 10$		
		265 (0.161) H-7 → L (0.49)		
exptl emiss λ_{max}	491	493	492	575
calcd λ_{max} [a]	471 (2.63 eV)	468 (2.65 eV)	468 (2.65 eV)	571 (2.17 eV)
T_1-S_0	441 H-2 ← L (0.66)	442 H-2 ← L (0.66)	441 H-4 ← L (0.51) H ← L (0.41)	518 H-2 ← L (0.73)

[a] Solvent-corrected (CH_2Cl_2) energy difference between the optimized ground state and lowest triplet state.

molecular structures of the electronic ground states and lowest triplet states of compounds **1a**, **1b**, **1e**, and **4a** were exemplarily studied. On the basis of the optimized geometries, time-dependent DFT (TD-DFT) calculations[37] combined with the conductive polarizable continuum model (CPCM)[38,39] were used to produce the molecular orbital energy levels and compositions, the absorption spectra, and the lowest singlet−singlet and singlet−triplet electronic transitions in CH_2Cl_2 media.

Selected TD-DFT singlet−singlet electronic transitions, excitation energies, and oscillator strengths of **1a**, **1b**, **1e**, and **4a** are given in Table 3. For **1a**, the lowest lying absorption transition $S_0 \rightarrow S_3$ at 318 nm ($f < 0.175$, the oscillator strengths for the $S_0 \rightarrow S_1$ and $S_0 \rightarrow S_2$ transitions being very small: $f < 0.005$) is in good agreement with the low-energy absorption band experimentally centered at 318 nm. This transition is derived from the HOMO-2 → LUMO excitation. As shown in Figure 4, both frontier orbitals are distributed predominantly over the organic ligand ppy (about 90%) with some contributions from the metal center and the alkynyl ligands (see Supporting Information for molecular orbital compositions). The absorption band can then be ascribed to a transition with a metal-perturbed intraligand charge-transfer $^1IL_{\pi\rightarrow\pi^*(ppy)}CT$ character. Other significant higher transitions at 292 nm ($S_0 \rightarrow S_4$, $f = 0.192$), 278 nm ($S_0 \rightarrow S_6$, $f = 0.123$), and 274 nm ($S_0 \rightarrow S_9$, $f = 0.311$) are better related to the intense high-energy band centered around 250−260 nm. They involve frontier molecular orbitals located either on the alkynyl ligands (HOMO-1, HOMO, and LUMO+2) or on the phenylpyridine (HOMO-3 and LUMO) with a small contribution from the metal center (less than 5%)

dx.doi.org/10.1021/ic102216v |*Inorg. Chem.* 2011, 50, 5430–5441

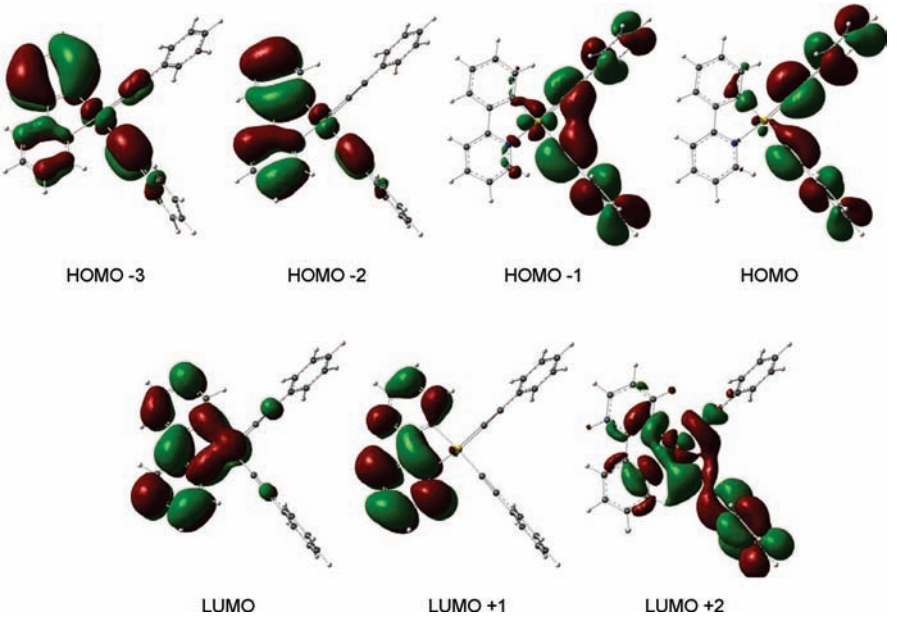

Figure 4. Isodensity plots of selected frontier orbitals of the ground state of **1a** (isodensity value, 0.02).

except for LUMO+2, which displays 25% of the electron density on the gold atom (Figure 4). The corresponding absorption band can be characterized as a transition with an admixture of intraligand charge-transfer $^1IL_{\pi\rightarrow\pi^*(ppy)}CT$ and metal-perturbed ligand-to-ligand $^1LL_{\pi(alk)\rightarrow\pi^*(alk)}CT$ characters.

For **1b**, the lowest significant singlet−singlet transitions $S_0 \rightarrow S_2$, $S_0 \rightarrow S_3$, and $S_0 \rightarrow S_4$ (f = 0.083, 0.182, 0.181; $S_0 \rightarrow S_1$ with $f < 0.010$) at 339, 318, and 292 nm are derived from the HOMO-1 → LUMO, HOMO-2 → LUMO, and HOMO-3 → LUMO excitations, respectively. Except HOMO-1 which is mainly located on the alkynyl ligands with a small contribution of the metal, the other four orbitals are a π/π^* combination of the phenylpyridine ligand. The main absorption band experimentally observed at 318 nm can be attributed to these three transitions characterized by metal-perturbed intraligand charge-transfer $^1IL_{\pi\rightarrow\pi^*(ppy)}CT$ and ligand-to-ligand $^1LL_{\pi(alk)\rightarrow\pi^*(ppy)}CT$ characters. The calculated electronic transitions for compound **1e** show the same general picture as that for **1b**. The influence of the terminal F atom in **1b** and the $SiMe_3$ group in **1e** on the alkynyl ligands is established by the lowest and significant singlet−singlet $\pi(alk) \rightarrow \pi^*(ppy)$ transitions with f = 0.083 and 0.079 at 339 and 323 nm, respectively. Nevertheless, the main character of the lowest absorption band of **1e** remains $\pi \rightarrow \pi^*(ppy)$ as shown by the $S_0 \rightarrow S_4$ and $S_0 \rightarrow S_5$ transitions calculated at 302 and 299 nm with the larger oscillator strengths f = 0.150 and 0.215, respectively. Compound **4a** differs from **1b** by the presence of 2-(2-thienyl)pyridine (thpy) instead of phenylpyridine. Experimentally, thpy is responsible of a lower energy absorption band at 368 nm for **4a** in comparison with **1a**−**1f**. The lowest transitions at 353, 351, and 337 nm calculated for **4a** (f = 0.038, 0.138, 0.267) are in good agreement with the experimental trend. As in **1a**, **1b**, and **1e**, the LUMO is localized on the N^C ligand with a small contribution from the metal center. HOMO and HOMO-1 are π-alkynyl based orbitals, and HOMO-2 distributes over thpy; consequently the corresponding HOMO → LUMO, HOMO-2 → LUMO, and HOMO-1 → LUMO excitations give rise to the main experimental absorption bands with an admixture of the metal-perturbed $^1IL_{\pi\rightarrow\pi^*(thpy)}CT$ and $^1LL_{\pi(alk)\rightarrow\pi^*(thpy)}CT$ characters.

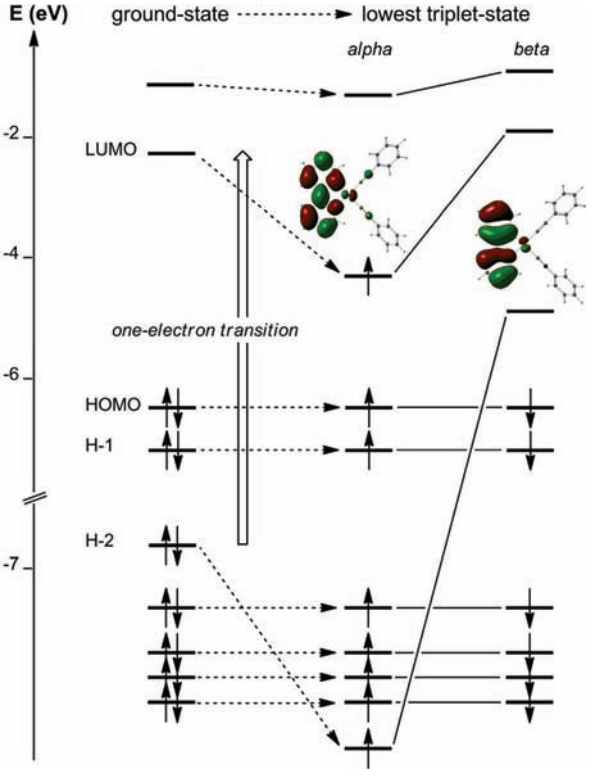

Figure 5. MO diagrams for the ground state and lowest triplet state of **1a**.

It is worth noting that the lowest TD-DFT excited states are calculated to be of triplet character at 441, 442, 441, and 518 nm for **1a**, **1b**, **1e**, and **4a**, respectively (Table 3). These calculated transitions are not observed in the visible region of the experimental absorption spectra, confirming the spin-forbidden character of these singlet−triplet transitions. For all compounds the calculated wavelengths corresponding to the $T_1 \rightarrow S_0$ transitions

dx.doi.org/10.1021/ic102216v |*Inorg. Chem.* 2011, 50, 5430–5441

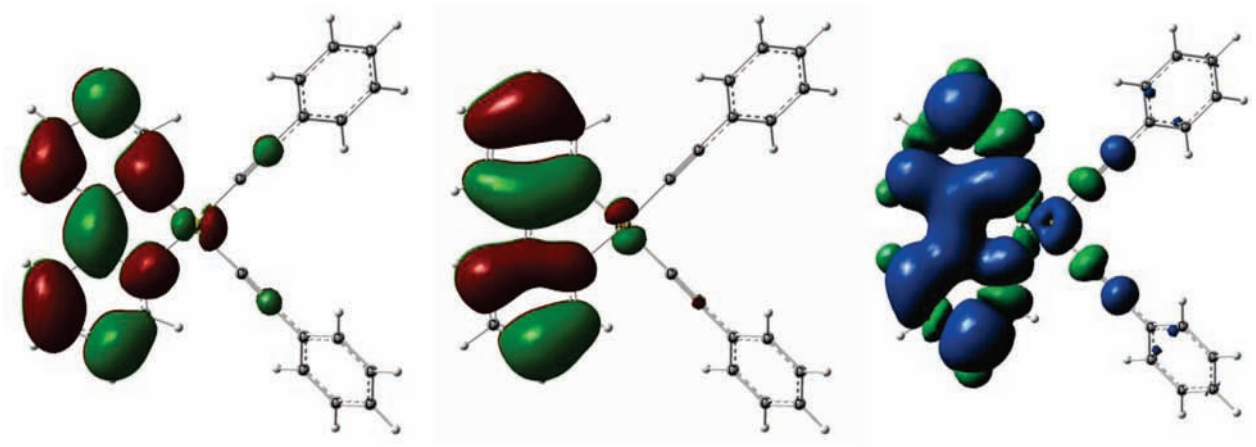

Figure 6. Isodensity plots of the singlet HOMO (left), singlet LUMO (middle), and the triplet spin density surface of the lowest triplet state of **1a** (isodensity value, 0.02).

are in line with the experimental emission wavelengths (in parentheses) with 441 (491), 442 (493), 441 (492), and 518 (575) nm for **1a**, **1b**, **1e**, and **4a**, respectively (Table 3). Nevertheless, the calculated emission maxima are more reliable when based on the energy difference between the optimized emissive triplet state and the optimized ground state. Indeed, the calculated values reported in Table 3 as calculated λ_{max} of 471 (**1a**), 468 (**1b**), 468 (**1e**), and 571 (**4a**) are in good agreement with the experimental values even still underestimated by 4−25 nm. Careful analyses of the molecular orbital diagrams of the optimized closed-shell ground state and open-shell triplet state of **1a** (Figure 5) confirm that the calculated transition LUMO → HOMO-2 is responsible of the experimental emission at 491 nm. They also reveal some inversion in the order of the orbitals with geometrical consequences. The ground-state HOMO-2 (−6.90 eV) is greatly affected by the one-electron HOMO-2 → LUMO excitation since the derived singly occupied α orbital of the triplet state is found at −7.47 eV as HOMO-7(α) while the corresponding unoccupied β orbital is the singlet LUMO of the system (−4.83 eV). The population of the ground-state LUMO (−2.13 eV) by one electron stabilized the singlet molecular orbital which becomes HOMO(α) in the triplet -state MO diagram (at −4.22 eV), while the corresponding unoccupied orbital is only slightly destabilized as LUMO+1(β) at −1.91 eV (Figure 5). The electronic density of the HOMO-2 and LUMO being mainly localized on the phenylpyridine ligand with a π-antibonding character of the central C−C bridge for the former and contrastingly a π-bonding character of the central C−C bridge for the latter orbital, the main variation observed in the optimized excited state with respect to the ground-state geometry is a significant shortening of the central C−C bond by 0.076 Å (1.388 Å vs 1.464 Å). The singlet HOMO, singlet LUMO, and the triplet spin density surface of the lowest triplet state of **1a** (Figure 6) visually identify the emission from a transition with a ^{3}ILCT character originated by the phenylpyridine ligand. Comparable studies were carried out for the other selected compounds **1b**, **1e**, and **4a** with no major differences in comparison with **1a** since the frontier orbitals involved in the calculated emissions and the triplet spin density surfaces of the lowest triplet states are similar in shape. For all studied compounds, the calculated phosphorescences are the reverse processes of the lowest lying absorptions because of the same transition characters.

CONCLUSIONS

In conclusion, we have developed a facile synthetic access toward tunable phosphorescent gold(III) *cis*-dialkynyl complexes. As demonstrated, the method can be applied quite generally to various gold(III) cyclometalated complexes bearing different alkynyls. This might help further to understand fundamental photophysics associated with gold(III) alkynyl complexes and design molecules with increased quantum yields suitable for OLEDs. The basic square-planar gold(III) dialkynyl motif could also be advantageously used for the development of macromolecules which are limited until now as compared to the isoelectronic platinum(II) systems.

EXPERIMENTAL SECTION

Material and Methods. All manipulations were carried out without special precautions for excluding air and moisture. ^{1}H and ^{13}C{^{1}H} NMR were recorded on Bruker AV2-400 or AV-500 spectrometers. ^{19}F NMR spectra were recorded on either a Varian Mercury spectrometer or Bruker AV2-400 spectrometers. Chemical shifts (δ) are reported in parts per million (ppm) referenced to tetramethylsilane (δ 0.00 ppm) using the residual protio solvent peaks as internal standards (^{1}H NMR experiments) or the characteristic resonances of the solvent nuclei (^{13}C NMR experiments). ^{19}F NMR was referenced to $CFCl_3$ (δ 0.00 ppm). Coupling constants (J) are quoted in hertz, and the following abbreviations are used to describe the signal multiplicities: s (singlet); d (doublet); t (triplet); q (quartet); m (multiplet); dd (doublet of doublet); td (triplet of doublet); dt (doublet of triplet). Proton and carbon assignments have been made using routine one- and two-dimensional NMR spectroscopies where appropriate. Infrared (IR) spectra were recorded on a Perkin-Elmer 1600 Fourier transform spectrophotometer using KBr pellet with frequencies (ν) quoted in wavenumbers (cm^{-1}). Elemental microanalysis was carried out with a Leco CHNS-932 analyzer. Mass spectra were run on a Finnigan-MAT-8400 mass spectrometer. Thin-layer chromatography (TLC) analysis was performed on precoated Merck silica gel $60F_{254}$ slides and visualized by luminescence quenching either at (short wavelength) 254 nm or (long wavelength) 365 nm. Chromatographic purification of products was performed on a short column (length, 15.0 cm; diameter, 1.5 cm) using forced flow of eluent. UV−vis measurements were carried out on a Perkin-Elmer Lambda 19 UV/vis spectrophotometer. Emission spectra were acquired on Perkin-Elmer spectrophotometer using 450 W xenon lamp excitation by exciting at the longest wavelength absorption maxima. All samples for emission spectra

dx.doi.org/10.1021/ic102216v |*Inorg. Chem.* 2011, 50, 5430–5441

were degassed by at least three freeze−pump−thaw cycles in an anaerobic cuvette and were pressurized with N_2 following each cycle. Emission spectra at 77 K were acquired in frozen 2-methyltetrahydrofuran (2-me-THF) glass. Luminescence quantum yields (Φ_p) were determined at 298 K (estimated uncertainty, ±15%) using standard methods;[40] wavelength-integrated intensities (I) of the corrected emission spectra were compared to isoabsorptive spectra of quinine sulfate standard (Φ_{ref} = 0.546 in 1 N H_2SO_4 air-equilibrated solution) and was corrected for solvent refractive index. Phosphorescence lifetimes were measured by time-correlated single-photon counting method (TCSPC) performed on an Edinburgh FLS920 spectrophotometer, using nF900 lamp source at 30 000 Hz frequency with 15 nm excitation and 15 nm emission slit widths. Thermogravimetric analysis (TGA) was done using a NETZSCH STA 449C instrument. Cyclic voltammograms were obtained with BAS 100W voltammetric analyzer. The cell was equipped with a gold working electrode, a Pt counter electrode, and a nonaqueous reference electrode. All sample solutions (CH_2Cl_2) were approximately 5×10^{-3} M in substrate and 0.1 M in Bu_4NPF_6 and were prepared under nitrogen. Ferrocene was subsequently added and the calibration of voltammograms recorded. The BAS 100W program was employed for data analysis.

Commercially available reagents were purchased from Aldrich and were used as such without further purification. Sodium tetrachloroaurate-(III) dihydrate was purchased from Strem Chemicals. All terminal alkynes described were either commercially purchased or synthesized by established sonogashira cross-coupling protocol.

*Synthesis of [(N^C)AuCl$_2$] [N^C = 2-(2,4-Difluorophenyl)pyridine] (**D**).* (3,5-Difluoro-2-(pyridin-2-yl)phenyl)mercury(II) chloride (0.170 g, 0.398 mmol) was added as a suspension in dichloromethane (DCM) (15.0 mL) to a solution of sodium tetrachloroaurate(III) dihydrate (0.158 g, 0.397 mmol) in acetonitrile (15.0 mL), and the mixture was stirred for 4 h at RT. It was then filtered and washed with cold acetonitrile (4.0 mL) and dried in vacuo to obtain off-white solid. Yield = 0.087 g, 48%. Positive ESI-MS: m/z 421.0 $[M - Cl]^+$. IR (KBr): ν(Au−Cl) 301, 320 cm^{-1}. ^1H NMR (500 MHz, DMSO-d_6, 298 K): δ 7.35 (td, J = 10.0 Hz, 2.5 Hz, 1H), 7.53 (d, J = 7.0 Hz, 1H), 7.77 (t, J = 7.0 Hz, 1H), 8.26 (d, J = 8.0 Hz, 1H), 8.37 (t, J = 7.5 Hz, 1H), 9.61 (d, J = 7.0 Hz, 1H). $^{13}C\{^1H\}$ NMR (125 MHz, DMSO-d_6, 298 K): δ 105.2 (t, $^2J_{C-F}$ = 26.0 Hz), 113.5 (d, $^2J_{C-F}$ = 26.0 Hz), 124.3 (d, $^2J_{C-F}$ = 19.5 Hz), 125.1, 127.0, 144.4, 148.4, 150.3, 158.8 (dd, $^1J_{C-F}$ = 260.0 Hz, 12.3 Hz), 160.5, 161.2 (dd, $^1J_{C-F}$ = 260.0 Hz, 12.5 Hz). ^{19}F NMR (282 MHz, DMSO-d_6, 298 K): δ −107.0, −102.2. Anal. Calc for $C_{11}H_6AuCl_2F_2N$ (%): C, 28.84; H, 1.32; N, 3.06. Found: C, 28.62; H, 1.26; N, 3.19.

*Synthesis of [(N^C)AuCl$_2$] [N^C = Benzo[h]quinoline][AuCl$_2$] (**E**).* Benzo[h]quinolin-10-ylmercury(II) chloride (0.15 g, 0.362 mmol) in DCM (20 mL) was added to a solution of sodium tetrachloroaurate(III) dihydrate (0.143 g, 0.360 mmol) in acetonitrile (20 mL), and the mixture was refluxed for 4 days. The pale violet solid that separated out was collected by filtration, washed with cold acetonitrile (15 mL), and dried under reduced pressure. Yield = 0.093 g, 58%. Positive ESI-MS: m/z 467.8 $[M + Na]^+$. IR (KBr): ν(Au−Cl) 378, 412 cm^{-1}. ^1H NMR (400 MHz, DMSO-d_6, 298 K): δ 7.71 (t, J = 7.5 Hz, 1H), 7.80 (d, J = 7.5 Hz, 1H), 7.9−8.0 (m, 4H), 8.93 (d, J = 8.5 Hz, 1H), 9.63 (d, J = 5.6 Hz, 1H); $^{13}C\{^1H\}$ NMR (125 MHz, DMSO-d_6, 298 K): δ 125.1, 126.3, 128.5, 128.9, 129.0, 130.0, 130.3, 131.4, 136.3, 143.4, 149.0, 152.2, 155.7. Anal. Calc for $C_{13}H_8AuCl_2N$ (%): C, 35.00; H, 1.81; N, 3.14. Found: C, 34.79; H, 1.83; N, 2.97.

*General Procedure for the Synthesis of Cyclometalated Gold(III) σ-Dialkynyl Complexes (**1a**−**1f**, **2a**, **3a**, **4a**, and **5a**).* To the suspension of respective cycloaurated gold(III) dichlorides (1.0 equiv.) in DCM (ca. 5.0 mL) are sequentially added the corresponding alkynes (2.3 equiv), triethylamine (0.055 equiv), and CuI (0.15 equiv) at RT. The suspension quickly turns into clear homogeneous solution, which is then further stirred for 15 min. Removal of solvents in vacuo, followed by sufficient pentane wash, yields the crude material. Purification by flash column chromatography (neutral Al_2O_3:eluent:EtOAc and hexane mixture) yields respective products as off-white to yellow solids. In some cases the purification procedures are slightly modified and are described below individually along with characterization data.

Note: During initial optimization experiments, aqueous workup protocol was followed and compounds were found to be quite stable to addition of water; later a direct purification procedure as described above was adopted because it gave improved yields.

*Synthesis of [(N^C)AuL$_2$] [N^C = 2-Phenylpyridine, L = Phenylacetylene] (**1a**).* The reaction of **A** (0.10 g, 0.236 mmol) with phenylacetylene (0.06 mL, 0.538 mmol) following the general procedure yielded **1a** as an off-white solid after column chromatography (neutral Al_2O_3; eluent, hexane/EtOAc = 5:1). Yield = 0.072 g, 55%. Positive ESI-MS: m/z 553.0 $[M^+]$. IR (KBr): ν(C≡C) 2132, 2160 cm^{-1}. ^1H NMR (500 MHz, $CDCl_3$, 298 K): δ 7.33−7.48 (m, 8H), 7.50−7.54 (m, 1H), 7.58−7.63 (m, 4H), 7.81 (d, J = 10.0 Hz, 1H), 8.02 (d, J = 10.0 Hz, 1H), 8.16 (t, J = 10.0 Hz, 1H), 8.32 (d, J = 10.0 Hz, 1H), 9.74 (d, J = 5.0 Hz, 1H). $^{13}C\{^1H\}$ NMR (125 MHz, $CDCl_3$, 298 K): δ 80.8, 99.5, 104.3, 118.3, 121.0, 124.8, 125.4, 126.4, 126.5, 127.6, 128.1, 128.7, 128.8, 132.2 (2C), 132.3, 132.4, 136.2, 142.3, 146.1, 151.4, 156.6, 167.4. Anal. Calc for $C_{27}H_{18}AuN$ (%): C, 58.60; H, 3.28; N, 2.53. Found: C, 58.39; H, 3.46; N, 2.40.

*Synthesis of [(N^C)AuL$_2$] [N^C = 2-Phenylpyridine, L = 1-Ethynyl-4-fluorobenzene] (**1b**).* The reaction of **A** (0.20 g, 0.473 mmol) with 1-ethynyl-4-fluorobenzene (0.124 mL, 1.08 mmol) following the general procedure yielded **1b** as an off-white solid which was purified by column chromatography (neutral Al_2O_3; eluent, hexane/EtOAc = 1:1). Yield = 0.175 g, 63%. Positive ESI-MS: m/z 612.0 $[M + Na]^+$. IR (KBr): ν(C≡C) 2137, 2165 cm^{-1}. ^1H NMR (500 MHz, CD_2Cl_2, 298 K): δ 7.05−7.11 (m, 4H), 7.40−7.47 (m, 2H), 7.51 (t, J = 7.5 Hz, 1H), 7.55−7.61 (m, 4H), 7.78 (d, J = 7.5 Hz, 1H), 8.00 (d, J = 7.5 Hz, 1H), 8.14 (t, J = 7.5 Hz 1H), 8.25 (d, J = 10.0 Hz, 1H), 9.66 (d, J = 5.5 Hz, 1H). $^{13}C\{^1H\}$ NMR (125 MHz, $CDCl_3$, 298 K): δ 79.6, 97.8, 102.6, 115.1, 115.3, 117.1, 120.5, 121.9, 122.0, 124.3, 124.9, 127.6, 131.8, 133.4, 133.5, 135.6, 141.8, 145.5, 150.9, 155.8, 162.0 (d, $^1J_{C-F}$ = 246.0 Hz), 161.7 (d, $^1J_{C-F}$ = 246.0 Hz), 166.8. ^{19}F NMR (282 MHz, CD_2Cl_2, 298 K): δ −115.3, −114.9. Anal. Calc for $C_{27}H_{16}AuF_2N$ (%): C, 55.02; H, 2.74; N, 2.38. Found: C, 54.94; H, 2.70; N, 2.25.

*Synthesis of [(N^C)AuL$_2$] [N^C = 2-Phenylpyridine, L = 5-Ethynyl-1,2,3-trimethoxybenzene] (**1c**).* The reaction of **A** (0.10 g, 0.236 mmol) with 5-ethynyl-1,2,3-trimethoxybenzene (0.104 g, 0.542 mmol) following the general procedure yielded **1c** as a yellow crystalline solid after chromatographic purification (neutral Al_2O_3; eluent, hexane/EtOAc = 1:1). Yield = 0.089 g, 50%. IR (KBr): ν(C≡C) 2161, 2171 cm^{-1}. ^1H NMR (500 MHz, CD_2Cl_2, 298 K): δ 3.82 (s, 6H), 3.83 (s, 6H), 3.89 (s, 3H), 3.90 (s, 3H), 6.84 (s, 2H), 6.86 (s, 2H), 7.41−7.49 (m, 2H), 7.53 (t, J = 10.0 Hz, 1H), 7.80 (d, J = 10.0 Hz, 1H), 8.00 (d, J = 10.0 Hz, 1H), 8.16 (t, J = 10.0 Hz, 1H), 8.28 (d, J = 5.0 Hz. 1H), 9.70 (d, J = 5.0 Hz, 1H). $^{13}C\{^1H\}$ NMR (125 MHz, CD_2Cl_2, 298 K): δ 56.0, 60.5, 79.0, 99.0, 103.9, 108.8, 108.9, 116.4, 120.5, 120.7, 120.9, 124.3, 124.9, 127.6, 128.5, 131.6, 135.6, 138.0, 138.2, 141.8, 142.5, 145.5, 147.8, 150.8, 153.0, 155.9, 166.7. Anal. Calc for $C_{33}H_{30}AuNO_6$ (%): C, 54.03; H, 4.12; N, 1.91. Found: C, 53.95; H, 4.01; N, 1.78.

*Synthesis of [(N^C)AuL$_2$] [N^C = 2-Phenylpyridine, L = 2-Ethynylthiophene] (**1d**).* The reaction of **A** (0.10 g, 0.236 mmol) with 2-ethynylthiophene (0.058 g, 0.542 mmol) following the general procedure yielded **1d** as a light brown solid after successive purification by column chromatography (neutral Al_2O_3; eluent, hexane/EtOAc = 2:1), and crystallization at −30 °C in DCM/pentane mixtures (1:1). Yield = 0.033 g, 25%. IR (KBr): ν(C≡C) 2145, 2155 cm^{-1}. ^1H NMR (500 MHz, $CDCl_3$, 298 K): δ 6.95 (dt, J = 9.0 Hz, 3.2 Hz, 2H), 7.13−7.21 (m, 3H), 7.30−7.37 (m, 3H), 7.47 (t, J = 5.5 Hz, 1H), 7.78 (d, J = 7.5 Hz, 1H), 7.79 (d, J = 7.5 Hz, 1H), 8.05 (t, J = 5.0 Hz, 1H), 8.09 (d, J = 5.2 Hz, 1H), 9.5 (d, J = 5.5 Hz, 1H). $^{13}C\{^1H\}$ NMR (125 MHz, $CDCl_3$, 298 K):

δ 85.2, 91.3, 96.1, 98.4, 120.6, 122.7, 124.3, 125.1, 125.2, 125.8, 126.0, 126.2, 126.8, 127.7, 130.5, 130.9, 131.7, 135.4, 141.8, 145.3, 150.7, 155.4, 166.5. Anal. Calc for $C_{23}H_{14}AuNS_2$ (%): C, 48.85; H, 2.50; N, 2.48. Found: C, 48.61; H, 2.44; N, 2.42.

*Synthesis of [(N^C)AuL$_2$] [N^C = 2-Phenylpyridine, L = Ethynyltrisopropylsilane] (**1e**).* The reaction of **A** (0.072 g, 0.170 mmol) with ethynyltrisopropylsilane (0.088 mL, 0.390 mmol) following the general procedure yielded **1e** as a white crystalline solid after chromatographic purification. (neutral Al_2O_3; eluent, hexane/EtOAc = 2:1). Yield = 0.072 g, 60.0%. Positive EI-MS: m/z 736.3 $[M + Na]^+$. IR (KBr): ν(C≡C) 2095, 2071 cm^{-1}. ^1H NMR (500 MHz, CD_2Cl_2, 298 K): δ 1.14 (s, 18H), 1.17 (s, 18H), 1.22 (s, 3H), 1.23 (s, 3H), 7.40−7.45 (m, 3H), 7.74 (d, J = 7.5 Hz, 2.0 Hz 1H), 7.96 (d, J = 7.5 Hz, 1H), 8.10 (t, J = 7.5 Hz, 1H), 8.31 (dd, J = 7.5 Hz, 2.0 Hz, 1H), 9.78 (d, J = 7.5 Hz, 1H). $^{13}C\{^1H\}$ NMR (125 MHz, CD_2Cl_2, 298 K): δ 11.6, 11.7, 18.6, 18.7, 96.6, 99.0, 102.8, 120.2, 123.7, 124.6, 127.3, 131.3, 136.0, 138.0, 141.7, 145.5 150.7, 156.4, 166.8. Anal. Calc for $C_{33}H_{50}AuNSi_2$ (%): C, 55.52; H, 7.06; N, 1.96. Found: C, 55.60; H, 6.96; N, 1.76.

*Synthesis of [(N^C)AuL$_2$] [N^C = 2-Phenylpyridine, L = 1-Ethynyl-4-(phenylethynyl)benzene] (**1f**).* The reaction of **A** (0.10 g, 0.236 mmol) with 1-ethynyl-4-(phenylethynyl)benzene (0.109 g, 0.542 mmol) following the general procedure yielded **1f** as a yellow solid which was further purified by column chromatography (acidic Al_2O_3; eluent, hexane/EtOAc = 2:1). Yield = 0.1 g, 56.0%. IR (KBr): ν(C≡C) 2129, 2159 cm^{-1}. ^1H NMR (500 MHz, $CDCl_3$, 298 K): δ 7.41−7.44 (m, 7H), 7.45−7.62 (m, 14H), 7.81 (d, J = 10.0 Hz, 1H), 8.02 (d, J = 10 Hz, 1H), 8.17 (t, J = 10 Hz, 1H), 8.27 (d, J = 5.5 Hz, 1H), 9.70 (d, J = 5.5 Hz, 1H). $^{13}C\{^1H\}$NMR (125 MHz, CD_2Cl_2, 298 K): δ 82.8, 89.2, 90.5, 98.8, 103.6, 120.7, 120.3, 120.5, 121.6, 122.0, 123.0, 124.2, 124.4, 124.5, 124.9, 125.2, 125.8, 125.9, 127.4, 127.6, 128.4, 128.5, 131.1, 131,3, 131.5, 131.6, 131.7, 131.7, 131.9, 135.6, 141.9, 145.5, 150.9, 156.7, 166.9. Anal. Calc for $C_{43}H_{26}AuN$ (%): C, 68.53; H, 3.48; N, 1.86. Found: C, 68.56; H, 3.58; N, 1.62.

*Synthesis of [(N^C)AuL$_2$] [N^C = 2-(2,4-Difluorophenyl)pyridine, L = Phenylacetylene] (**2a**).* The reaction of **D** (0.060 g, 0.131 mmol) with phenylacetylene (0.032 mL, 0.298 mmol) following the general procedure yielded **2a** as an off-white solid after chromatographic purification (neutral Al_2O_3; eluent, hexane/EtOAc = 1:1). Yield = 0.032 g, 41%. IR (KBr): ν(C≡C) 2137, 2165, cm^{-1}. ^1H NMR (500 MHz, CD_2Cl_2, 298 K): δ 6.86 (td, J = 8.0 Hz, 2.5 Hz, 1H), 7.30−7.39 (m, 6H), 7.50 (t, J = 8.0 Hz, 1H), 7.59−7.64 (m, 4H), 7.97 (dd, J = 8.0 Hz, 2.5 Hz, 1H), 8.14 (t, J = 7.5 Hz, 1H), 8.35 (d, J = 8.0 Hz, 1H), 9.80 (dd, J = 8.0 Hz, 2.5 Hz, 1H). $^{13}C\{^1H\}$ NMR (125 MHz, CD_2Cl_2, 298 K): δ 99.0, 103.8, 104.0 (t, $^2J_{C-F}$ = 26.2 Hz), 114.1, 118.8, 119.0, 124.2, 124.4, 124.6, 125.6, 125.8, 127.6, 127.9, 128.5, 128.6, 130.7, 132.0, 132.1, 142.7, 151.6, 161.2 (d, $^1J_{C-F}$ = 275.0 Hz), 163.9, 164.1(d, $^1J_{C-F}$ = 275.0 Hz). ^{19}F NMR (188 MHz, CD_2Cl_2, 298 K): δ −109.2, −105.4. Anal. Calc for $C_{27}H_{16}AuF_2N.H_2O$ (%): C, 53.39; H, 2.99; N, 2.31. Found: C, 53.20; H, 2.91; N, 2.31. (Note: The elemental analysis was measured on a sample obtained by aqueous workup which was confirmed to be identical to the above-described in all respects.)

*Synthesis of [(N^C)AuL$_2$] [N^C = Benzo[h]quinoline, L = Phenylacetylene] (**3a**).* The reaction of **E** (0.085 g, 0.190 mmol) with phenylacetylene (0.048 mL, 0.430 mmol) following the general procedure yielded **3a** as an off-white solid after chromatographic purification. (neutral Al_2O_3; eluent, hexane/EtOAc = 2:1). Yield = 0.070 g, 64.0%. IR (KBr): ν(C≡C) 2135, 2160 cm^{-1}. ^1H NMR (500 MHz, CD_2Cl_2, 298 K): δ 7.34−7.44 (m, 6H), 7.64−7.68 (m, 4H), 7.57−7.82 (m, 3H), 7.87 (d, J = 8.0 Hz, 1H), 7.94 (d, J = 8.5 Hz, 1H), 8.37 (d, J = 7.0 Hz, 1H), 8.60 (d, J = 8.0 Hz, 1H), 9.81 (d, J = 5.5 Hz, 1H). $^{13}C\{^1H\}$ NMR (125 MHz, $CDCl_3$, 298 K): δ 78.3, 99.0, 103.6, 116.2, 122.9, 123.9, 125.8, 125.9, 127.0, 127.4, 128.2, 128.2, 128.4, 130.2, 130.8, 131.6, 131.7, 131.8, 133.5, 134.8, 140.5, 141.2, 149.7, 154.7, 155.7. Anal. Calc for $C_{29}H_{18}AuN$ (%): C, 60.32; H, 3.14; N, 2.43. Found: C, 60.23; H, 3.27; N, 2.33.

*Synthesis of [(N^C)AuL$_2$] [N^C = 2-(2-Thienyl)pyridine, L = 1-Ethynyl-4-fluorobenzene] (**4a**).* The reaction of **B** (0.10 g, 0.233 mmol) with 1-ethynyl-4-fluorobenzene (0.061 mL, 0.532 mmol) following the general procedure yielded **4a** as an off-white solid after chromatographic purfication (neutral Al_2O_3; eluent, hexane/EtOAc = 1:1). Yield = 0.08 g, 57%. IR (KBr): ν(C≡C) 2120, 2160 cm^{-1}. ^1H NMR (500 MHz, $CDCl_3$, 298 K): δ 7.05−7.10 (m, 4H), 7.36 (t, J = 8.5 Hz, 1H), 7.54−7.64 (m, 7H), 8.05 (t, J = 8.5 Hz, 1H), 9.43 (d, J = 8.0 Hz, 1H). $^{13}C\{^1H\}$ NMR (125 MHz, $CDCl_3$, 298 K): δ 99.0, 102.8, 112.5, 115.1, 115.3, 119.6, 121.7, 122.0, 122.4, 130.0, 133.0, 133.4, 133.5, 133.6, 133.7, 142.3, 145.7, 150.5, 160.3, 161.9 ($^1J_{C-F}$ = 245.0 Hz), 162.4 ($^1J_{C-F}$ = 245.0 Hz). ^{19}F NMR (282 MHz, CD_2Cl_2, 298 K): δ −115.1, −114.8. Anal. Calc for $C_{25}H_{14}AuF_2NS$ (%): C, 50.43; H, 2.37; N, 2.35. Found: C, 50.35; H, 2.38; N, 2.22.

*Synthesis of [(N^C)AuL$_2$] [N^C = 2-(5-Methyl-2-thienyl)pyridine, L = 1-Ethynyl-4-fluorobenzene] (**5a**).* The reaction of **C** (0.178 g, 0.402 mmol) with 1-ethynyl-4-fluorobenzene (0.105 mL, 0.924 mmol) following the general procedure, but worked up after 5 min after addition of CuI, yielded **5a** as an off-white solid after chromatographic purification (neutral Al_2O_3; eluent, hexane/EtOAc = 1:1). Yield = 0.10 g, 41%. Positive EI-MS: m/z 632.1 $[M + Na]^+$. IR (KBr): ν(C≡C) 2129, 2165 cm^{-1}. ^1H NMR (500 MHz, CD_2Cl_2, 298 K): δ 2.62 (s, 3H), 7.05−7.10 (m, 4H), 7.16 (s, 1H), 7.27 (t, J = 8.5 Hz, 1H), 7.47 (d, J = 8.5, 1H) 7.54−7.58 (m, 4H), 8.05 (t, J = 8.5 Hz, 1H), 9.34 (d, J = 5.5 Hz, 1H). $^{13}C\{^1H\}$ NMR (125 MHz, $CDCl_3$, 298 K): δ 15.4, 71.4, 98.9, 102.2, 113.0, 115.1, 115.3, 118.8, 121.5, 121.7, 121.9, 131.5, 133.4, 133.7, 142.1, 143.1, 146.0, 150.2, 160.4, 161.3, 161.7 ($^1J_{C-F}$ = 267 Hz), 162.0 ($^1J_{C-F}$ = 248 Hz). ^{19}F NMR (188 MHz, CD_2Cl_2, 298 K): δ −115.1, −114.7. Anal. Calc for $C_{26}H_{16}AuF_2NS$ (%): C, 51.24; H, 2.65; N, 2.30. Found: C, 51.15; H, 2.77; N, 2.18.

Computational Details. All calculations were performed with the Gaussian 03 program package[36] using the hybrid functional PBE1PBE[41] in conjunction with the Stuttgart/Dresden effective core potentials (SDD) basis set[42] for the Au center augmented with one f-polarization function (exponent α = 1.050) and the standard 6-31+G(d) basis set[43] for the remaining atoms. Full geometry optimizations without symmetry constraints were carried out in the gas phase for the singlet ground states (S_0) and the lowest triplet excited states (T_1). The optimized geometries were confirmed to be potential energy minima by vibrational frequency calculations at the same level of theory, because no imaginary frequency was found. The first 10 singlet−singlet and singlet−triplet transition energies were computed at the optimized S_0 geometries, by using the time-dependent DFT methodology.[37] Solvent effects were taken into account using the conductor-like polarizable continuum model (CPCM)[39] with dichloromethane as solvent for single-point calculations on all optimized gas-phase geometries.

X-ray Diffraction Analyses. Relevant details about the structure refinements are given in Tables S1 and S2 of the Supporting Information, and selected geometrical parameters are included in Table 1 and the captions of the corresponding figures (Figures S2−S4 in the Supporting Information). Intensity data were collected at 183(2) K on an Oxford Xcalibur diffractometer (four-circle kappa platform, Ruby CCD detector, and a single-wavelength Enhance X-ray source with Mo Kα radiation; λ = 0.710 73 Å)[44] The selected suitable single crystals were mounted using polybutene oil on the top of a glass fiber fixed on a goniometer head and immediately transferred to the diffractometer. Preexperiment, data collection, data reduction, and analytical absorption corrections were performed with the Oxford program suite CrysAlisPro.[45] The crystal structures were solved with SHELXS-97[46] using direct methods. The structure refinements were performed by full-matrix least squares on F^2 with SHELXL-97.[46] All programs used during the crystal structure determination process are included in the WINGX software.[47] The program PLATON[48] was used to check the result of the X-ray analyses. CCDC-798717-798723 contains the supplementary crystallographic data

(excluding structure factors) for this paper. These data can be obtained free of charge from The Cambridge Crystallographic Data Center via www.ccdc.cam.ac.uk/data_request/cif.

■ ASSOCIATED CONTENT

Supporting Information. Text describing synthetic details and spectroscopic data of **D**, XRD details, and computational details as well as a reference list, figures showing step 1 for **D**, thermogravimetric analysis of **1a** and **1b**, ORTEP plots of **1b**, **1c**, and **4a**, absorption and emission spectra of **1b**−**1e** and **2a**, cyclic voltammograms of **1a**, **1b**, and **1d**, spatial plots, energies, and compositions of frontier molecular orbitals, singlet HOMO and LUMO of the lowest triplet state of **1a**, and triplet spin density surfaces, and tables listing crystallographic details of all X-ray structures (Table S1 and Table S2), summary of interplanar Au−Au distances, summary of cyclic voltammetry, and computational details and X-ray crystallographic data for complexes **1a**−**1c**, **1e**, **3a**, **4a**, and **5a** (pdf). This material is available free of charge via the Internet at http://pubs.acs.org.

■ AUTHOR INFORMATION

Corresponding Author
*E-mail: venkatesan.koushik@aci.uzh.ch.

■ ACKNOWLEDGMENT

We thank S. V. Rocha and Dr. N. Finney for help with lifetime measurements. K.V. is grateful to the University of Zürich and Prof. H. Berke for generous support.

■ REFERENCES

(1) Yam, V. W.-W.; Cheung, K. L.; Yip, S. K.; Cheung, K. K. *J. Organomet. Chem.* **2003**, *681*, 196–209.
(2) Yam, V. W.-W.; Wong, K. M.-C.; Hung, L.-L.; Zhu, N. Y. *Angew. Chem., Int. Ed.* **2005**, *44*, 3107–3110.
(3) Vicente, J.; Chicote, M. T.; Alvarez-Falcon, M. M.; Bautista, D. *Organometallics* **2004**, *23*, 5707–5712.
(4) Irwin, M. J.; Vittal, J. J.; Puddephatt, R. J. *Organometallics* **1997**, *16*, 3541–3547.
(5) Vicente, J.; Chicote, M. T.; Alvarez-Falcon, M. M.; Abrisqueta, M. D.; Hernandez, F. J.; Jones, P. G. *Inorg. Chim. Acta* **2003**, *347*, 67–74.
(6) Vicente, J.; Chicote, M. T.; Alvarez-Falcon, M. M.; Jones, P. G. *Chem. Commun. (Cambridge, U.K.)* **2004**, 2658–2659.
(7) Schuster, O.; Schmidbaur, H. *Inorg. Chim. Acta* **2006**, *359*, 3769–3775.
(8) Yam, V. W.-W. *Acc. Chem. Res.* **2002**, *35*, 555–563.
(9) Vicente, J.; Gil-Rubio, J.; Barquero, N.; Jones, P. G.; Bautista, D. *Organometallics* **2008**, *27*, 646–659.
(10) Johnson, A.; Puddephatt., R. J.; Quirk, J. L. *J. Chem. Soc., Chem. Commun.* **1972**, 938–939.
(11) Johnson, A.; Puddephatt, R. J. *J. Chem. Soc., Dalton Trans.* **1977**, 1384–1388.
(12) Wong, K. M.-C.; Hung, L. L.; Lam, W. H.; Zhu, N. Y.; Yam, V. W.-W. *J. Am. Chem. Soc.* **2007**, *129*, 4350–4365.
(13) Wong, K. M.-C.; Zhu, X. L.; Hung, L.-L.; Zhu, N. Y.; Yam, V. W.-W.; Kwok, H.-S. *Chem. Commun. (Cambridge, U.K.)* **2005**, 2906–2908.
(14) Schuster, O.; Liau, R. Y.; Schier, A.; Schmidbaur, H. *Inorg. Chim. Acta* **2005**, *358*, 1429–1441.
(15) Schuster, O.; Schmidbaur, H. *Organometallics* **2005**, *24*, 2289–2296.
(16) Méndez, L. A.; Jiménez, J.; Cerrada, E.; Mohr, F.; Laguna, M. *J. Am. Chem. Soc.* **2005**, *127*, 852–853.
(17) Luquin, A.; Cerrada, E.; Laguna, M., *Gold Chemistry—Applications and Future Directions in the Life Sciences*. Wiley-VCH: Weinheim, Germany, 2009.
(18) Chan, C.-W.; Wong, W.-T.; Che, C.-M. *Inorg. Chem.* **1994**, *33*, 1266–1272.
(19) Au, V. K.-M.; Wong, K. M.-C.; Tsang, D. P.-K.; Chan, M.-Y.; Zhu, N.; Yam, V. W.-W. *J. Am. Chem. Soc.* **2010**, *132*, 14273–14278.
(20) Yam, V. W.-W.; Tang, R. P.-L.; Wong, K. M.-C.; Lu, X.-X.; Cheung, K.-K.; Zhu, N. *Chem.—Eur. J.* **2002**, *8*, 4066–4076.
(21) Garg, J. A.; Blacque, O.; Fox, T.; Venkatesan, K. *Inorg. Chem.* **2010**, *49*, 11463–11472.
(22) (a) Au, V. K.-M.; Wong, K. M.-C.; Zhu, N. Y.; Yam, V. W.-W. *Chem.—Eur. J.* **2011**, *17*, 130–142. (b) Yam, V. W.-W.; Choi, S. W.-K.; Lai, T.-F.; Lee, W.-T. *J. Chem. Soc., Dalton Trans.* **1993**, 1001–1002.
(23) Constable, E. C.; Leese, T. A. *J. Organomet. Chem.* **1989**, *363*, 419–424.
(24) Fuchita, Y.; Ieda, H.; Wada, S.; Kameda, S.; Mikuriya, M. *J. Chem. Soc., Dalton Trans.* **1999**, 4431–4435.
(25) Black, D. S.; Deacon, G. B.; Edwards, G. L.; Gatehouse, B. M. *Aust. J. Chem.* **1993**, *46*, 1323–1336.
(26) Parish, R. V.; Wright, J. P.; Pritchard, R. G. *J. Organomet. Chem.* **2000**, *596*, 165–176.
(27) Kresge, A. J.; Pruszynski, P. *J. Org. Chem.* **1991**, *56*, 4811–4815.
(28) Fernández, S.; Forniés, J.; Gil, B.; Gómez, J.; Lalinde, E. *Dalton Trans.* **2003**, 822–830.
(29) Henderson, W. *Adv. Organomet. Chem.*, **2006**, *54*, 207−265, and references therein.
(30) Tsuboyama, A.; Iwawaki, H.; Furugori, M.; Mukaide, T.; Kamatani, J.; Igawa, S.; Moriyama, T.; Miura, S.; Takiguchi, T.; Okada, S.; Hoshino, M.; Ueno, K. *J. Am. Chem. Soc.* **2003**, *125*, 12971–12979.
(31) Thomas, S. W., III; Venkatesan, K.; Müller, P.; Swager, T. M. *J. Am. Chem. Soc.* **2006**, *128*, 16641–16648.
(32) Tang, W.-S.; Lu, X.-X.; Wong, K. M.-C.; Yam, V. W.-W. *J. Mater. Chem.* **2005**, *15*, 2714–2720.
(33) Li, J.; Djurovich, P. I.; Alleyne, B. D.; Yousufuddin, M.; Ho, N. N.; Thomas, J. C.; Peters, J. C.; Bau, R.; Thompson, M. E. *Inorg. Chem.* **2005**, *44*, 1713–1727.
(34) Brooks, J.; Babayan, Y.; Lamansky, S.; Djurovich, P. I.; Tsyba, I.; Bau, R.; Thompson, M. E. *Inorg. Chem.* **2002**, *41*, 3055–3066.
(35) Au, V. K.-M.; Wong, K. M.-C.; Zhu, N. Y.; Yam, V. W.-W. *J. Am. Chem. Soc.* **2009**, *131*, 9076–9085.
(36) Frisch, M. J.; Trucks, G. W.; Schlegel, H. B.; Scuseria, G. E.; Rob, M. A.; Cheeseman, J. R.; Montgomery, J. A., Jr.; Vreven, T.; Kudin, K. N.; Burant, J. C.; Millam, J. M.; Iyengar, S. S.; Tomasi, J.; Barone, V.; Mennucci, B.; Cossi, M.; Scalmani, G.; Rega, N.; Petersson, G. A.; Nakatsuji, H.; Hada, M.; Ehara, M.; Toyota, K.; Fukuda, R.; Hasegawa, J.; Ishida, M.; Nakajima, T.; Honda, Y.; Kitao, O.; Nakai, H.; Klene, M.; Li, X.; Knox, J. E.; Hratchian, H. P.; Cross, J. B.; Bakken, V.; Adamo, C.; Jaramillo, J.; Gomperts, R.; Stratmann, R. E.; Yazyev, O.; Austin, A. J.; Cammi, R.; Pomelli, C.; Ochterski, J. W.; Ayala, P. Y.; Morokuma, K.; Voth, G. A.; Salvador, P.; Dannenberg, J. J.; Zakrzewski, V. G.; Dapprich, S.; Daniels, A. D.; Strain, M. C.; Farkas, O.; Malick, D. K.; Rabuck, A. D.; Raghavachari, K.; Foresman, J. B.; Ortiz, J. V.; Cui, Q.; Baboul, A. G.; Clifford, S.; Cioslowski, J.; Stefanov, B. B.; Liu, G.; Liashenko, A.; Piskorz, P.; Komaromi, I.; Martin, R. L.; Fox, D. J.; Keith, T.; Al-Laham, M. A.; Peng, C. Y.; Nanayakkara, A.; Challacombe, M.; Gill, P. M. W.; Johnson, B.; Chen, W.; Wong, M. W.; Gonzalez, C.; Pople, J. A. *Gaussian 03*; Gaussian: Wallingford, CT, 2003.
(37) (a) Stratmann, R. E.; Scuseria, G. E.; Frisch, M. J. *J. Chem. Phys.* **1998**, *109*, 8218–8224. (b) Bauernschmitt, R.; Ahlrichs, R. *Chem. Phys. Lett.* **1996**, *256*, 454–464. (c) Casida, M. E.; Jamorski, C.; Casida, K. C.; Salahub, D. R. *J. Chem. Phys.* **1998**, *108*, 4439–4449.
(38) Barone, V.; Cossi, M. *J. Phys. Chem. A* **1998**, *102*, 1995–2001.
(39) Cossi, M.; Rega, N.; Scalmani, G.; Barone, V. *J. Comput. Chem.* **2003**, *24*, 669–681.
(40) Demas, J. N.; Crosby, G. A. *J. Phys. Chem.* **1971**, *75*, 991–1024.
(41) Adamo, C.; Barone, V. *J. Chem. Phys.* **1999**, *110*, 6158–6170.

(42) Dunning, T. H., Jr.; Hay, P. J. In *Modern Theoretical Chemistry*; Schaefer, H. F., III, Ed.; Plenum: New York, 1976; Vol. 3, pp 1− 28.
(43) Ditchfield, R.; Hehre, W. J.; Pople, J. A. *J. Chem. Phys.* **1971**, *54*, 724–728.
(44) *Xcalibur CCD System*; Oxford Diffraction: Abingdon, Oxfordshire, England, 2007.
(45) *CrysAlisPro*, Versions 1.171.32.34d-55; Oxford Diffraction: Abingdon, Oxfordshire, England.
(46) Sheldrick, G. M. *Acta Crystallogr., Sect. A* **2008**, *64*, 112–122.
(47) Farrugia, L. J. *J. Appl. Crystallogr.* **1999**, *32*, 837–838.
(48) Spek, A. L. *J. Appl. Crystallogr.* **2003**, *36*, 7–13.